Electronic Supplementary Information

Stepwise synthesis of Zr-based metal-organic frameworks: Incorporating trinuclear zirconocene-based metallo-pyridine ligand

Juan Zhu[a], Zhao-Yang Liu[a], Shuang-bao Li[*b], He Huang[a], Bao-Xu Jiang[a], and Yu-Teng Zhang[*a]

[a]*College of Chemical Engineering, Northeast Electric Power University, Jilin City 132012, PR China.*

[b]*School of Chemical and Pharmaceutical Engineering, Jilin Institute of Chemical Technology, Jilin, 132022, PR China.*

*Corresponding author.

E-mail address: zhangyuteng@neepu.edu.cn; lishb997@nenu.edu.cn

Table S1. Typical ZrMOF materials based on the stepwise synthesis.

ZrMOFs	Precursor	Reactant (Metal)	Reactant (Ligand)	Reactant (Others)	Year	Ref.
Zirconium muconate	Zr_6 methacrylate cluster	/	muconic acid	/	2010	1
UiO-66 terephthalate	Zr_6 cluster	/	terephthalic acid	/	2010	1
SALI-PPA	NU-1000	/	/	PPA solutions	2019	2
PCN-160-$CoCl_2$	PCN-160-imine	$CoCl_2$	/	/	2018	3
PCN-161-$Co(OH)_2$	PCN-160-imine	$Co(OH)_2$	/	/	2018	3
PCN-161-$FeCl_2$	PCN-160-imine	$FeCl_2$	/	/	2018	3
UiO-68-M	UiO-68-Me	/	H_2L^M	/	2018	4
PCN-134	Zr-BTB	/	H_4ETTC	/	2018	5
PCN-222@MOF-5	PCN-222	/	/	$Zn(NO_3)_2·6H_2O$,H_2BDC	2018	6
PCN-900(Eu)-MTCPP	PCN-900(Eu)	$MCl_2·4H_2O$ (M = Zn, Fe, Ni, Co)	/	/	2018	7
PCN-900(Eu)-TCPP-BPDC	PCN-900(Eu)	/	H_2BPDC	/	2018	7
PCN-161	PCN-160	/	H_2CBAB	/	2019	8
UiO-68	PCN-161	/	H_2TPDC	/	2019	8
UiO-67	PCN-161	/	H_2BPDC	/	2019	8
M/Zr-bimetallic MOF	Zr-MOF	transition metal cations (M^{n+})	/	/	2019	9
PCN-608	$Zr_6O_4(OH)_4$ cluster	/	/	TCPB-OH, benzoic acid	2020	10
JMOF-1	Zr_3 cluster	PbI_2	/	/	2021	11
JMOF-2	Zr_3 cluster	$Pb(NO_3)_2$	/	/	2021	11
ZrMOF-Co/Ni	Zr_3 cluster	$CoCl_2·6H_2O$ $NiCl_2·6H_2O$	/	/	/	This work

1. Materials and Methods

All the reagents were obtained from commercial sources and used without further purification. Powder X-ray diffraction (PXRD) measurement was recorded ranging from 5 to 50º at room temperature on a Siemens D5005 diffractometer with Cu-Kα (λ = 1.5418 Å).The C, H, and N elemental analyses were conducted on a Perkin-Elmer 2400CHN elemental analyzer. Thermogravimetric analysis (TGA) of the samples was performed using a Perkin-Elmer TG-7 analyzer heated from room temperature to 800 ºC under nitrogen at the heating rate of 10 °C·min^{-1} . The C, H, and N elemental analyses were conducted on a Perkin-Elmer 2400CHN elemental analyzer. IR spectrum was performed in the range 4000–400 cm^{-1} using KBr pellets on an Alpha Centaurt FT/IR spectrophotometer. X-ray photoelectron spectroscopy analyses were performed on a VG ESCALABMKII spectrometer with an Al-Kα (1486.6 eV) achromatic X-ray source. The vacuum inside the analysis chamber was maintained at 6.2×10^{-6} Pa during the analysis.

2. Synthesis

2.1 Synthesis of the trinuclear zirconocene-based tripodal metallo-pyridine

The synthetic process of trinuclear zirconocene-based metallo-pyridine precursor was slightly modified according to the literature[11,12]. Sodium hydroxide (210 mg) was added a suspended aqueous solution of isonicotinic acid (615 mg, 15 mL water) to dissolve isonicotinic acid completely. Then, the pH of the solution was adjusted to be 6~7 by adding 2 M dil. HCl. The clear solution was then added dropwise to a solution of Cp_2ZrCl_2 (1.465 g) in dichloromethane (35 mL) with stirring. Subsequently, white precipitate appeared immediately. Keep stirring for more than two hours to ensure complete precipitation. After completion, the reaction mixture was filtered and washed with distilled water to obtain white solid (namely Zr_3 precursor) which was dried under vacuum at 60 °C.

2.2 Synthesis of Zr-MOF-Co and Zr-MOF-Ni

(1) Preparation of Zr-MOF-Co

Zr_3 precursor (70 mg) and $CoCl_2·6H_2O$ (10 mg) were added in 1 mL DMA (N,N' -dimethylformamide). Then the mixture was sealed in a vial and heated at 70 °C for 12h, then it was gradually cooled to room temperature, resulting in pink crystals that were isolated by washing with DMA and dried under vacuum at 30 °C. The yield based on Zr_3 precursor is 45%. Anal. Calcd: C, 40.3; H, 4.37; N,5.73. Found: C, 40.35; H, 4.33; N, 5.76. IR (KBr, cm^{-1}): 3300 (br),

1627 (s), 1542 (s), 1261 (w), 607 (s).

(2) Preparation of Zr-MOF-Ni

A 70 mg amount of Zr_3 precursor and $NiCl_2 \cdot 6H_2O$ (10 mg) was used in the same procedure as for **Zr-MOF-Co**. The mixture was dissolved in DMA (1 mL) and heated at 70 °C for 12h. Finally, colorless crystals were obtained by washing with DMA and dried under vacuum at 30 °C. The yield based on Zr_3 precursor is 40%. Anal. Calcd: C, 34.39; H, 4.43; N, 4.89. Found: C, 34.35; H, 4.47; N, 4.87. IR (KBr, cm^{-1}): 3300 (br), 1627 (s), 1541 (s), 1411 (s), 1259 (w), 609 (s).

Table S2. Crystallographic Data for **ZrMOF-Co and ZrMOF-Ni.**

	ZrMOF-Co	**ZrMOF-Ni**
Empirical formula	$C_{82}H_{106}Cl_4CoN_{10}O_{29}Zr_6$	$C_{82}H_{126}Cl_4N_{10}NiO_{54}Zr_6$
Formula weight	2443.85	2863.76
Temperature/K	150.0	150.0
Crystal system	triclinic	triclinic
Space group	P-1	P-1
a/Å	11.3034(6)	11.3213(6)
b/Å	12.7188(6)	12.5450(7)
c/Å	21.9772(12)	21.9866(13)
α/°	82.236(2)	82.573(2)
β/°	76.045(2)	76.173(2)
γ/°	75.545(2)	75.347(2)
Volume/$Å^3$	2959.8(3)	2925.7(3)
Z	1	1
$\rho_{calc}g/cm^3$	1.321	1.336
μ/mm^{-1}	0.795	0.823
F(000)	1185	1186
Radiation	MoKα (λ = 0.71073)	MoKα (λ = 0.71073)
2θ range for data collection/°	3.832 to 52.806	3.808 to 52.83
Index ranges	-14 ≤ h ≤ 14, -15 ≤ k ≤ 15, -27 ≤ l ≤ 27	-14 ≤ h ≤ 14, -15 ≤ k ≤ 15, -27 ≤ l ≤ 27
Reflections collected	91794	75035
Independent reflections	12099 [Rint = 0.0976, Rsigma = 0.0504]	11964 [Rint = 0.0824, Rsigma = 0.0488]
Data/restraints/parameters	12099/0/580	11964/0/592
Goodness-of-fit on F^2	1.091	1.066
Final R indexes [I>=2σ (I)]	R1 = 0.0530, wR2 = 0.1519	R1 = 0.0480, wR2 = 0.1392
Final R indexes [all data]	R1 = 0.0727, wR2 = 0.1694	R1 = 0.0674, wR2 = 0.1587

Largest diff. peak/hole / e $Å^{-3}$	0.82/-0.70	0.77/-1.02

Disordered solvent H_2O molecules were treated with the SQUEEZE program and included in molecular formula.

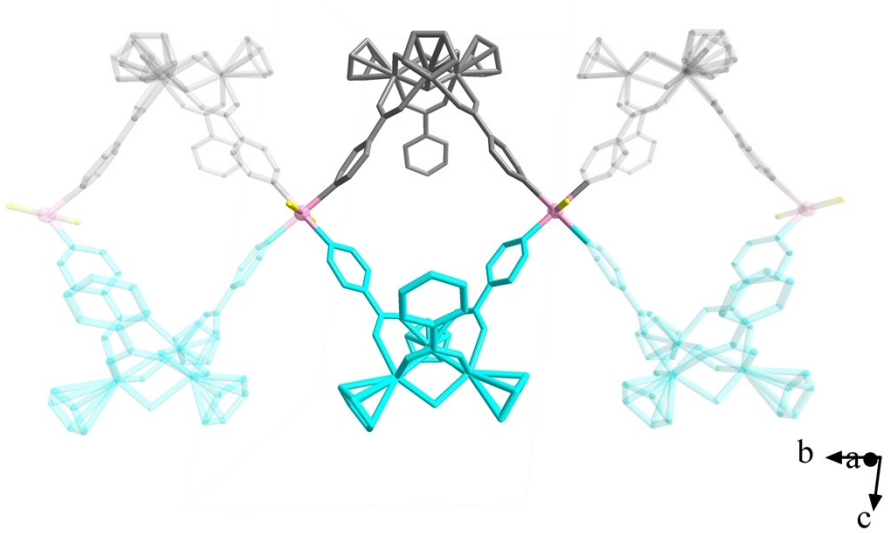

Figure S1. The crystal structure of **ZrMOF-Co/Ni**, highlighting the 2D infinite chain structure.

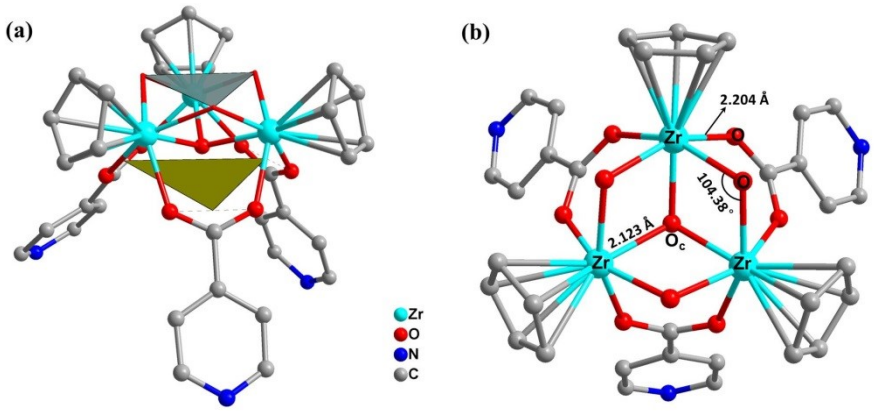

Figure S2. Trinuclear zirconocene-based metallo-pyridine buliding block. (a) highlighting the C_{3v}-symmetry; (b) the main bond angle and bond lengths.

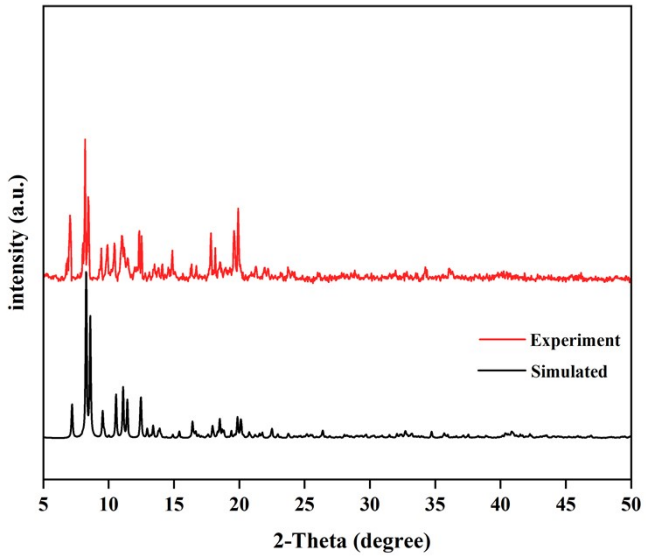

Figure S3. Experimental and simulated powder X-Ray diffraction patterns for **ZrMOF-Co**.

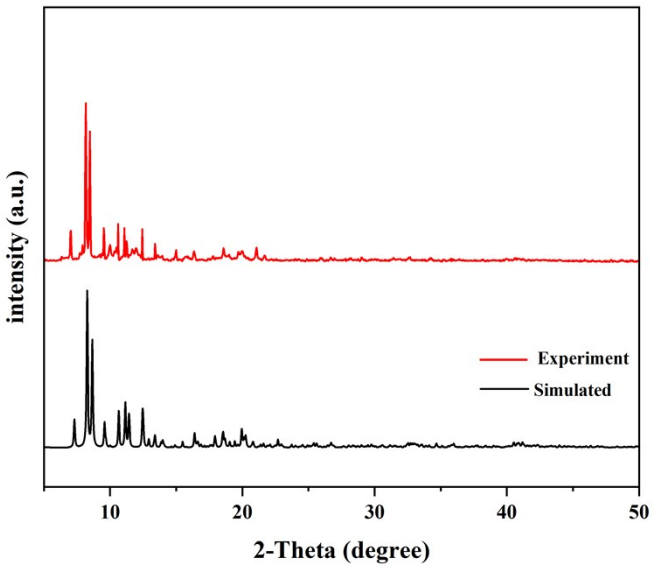

Figure S4. Experimental and simulated powder X-Ray diffraction patterns for **ZrMOF-Ni**.

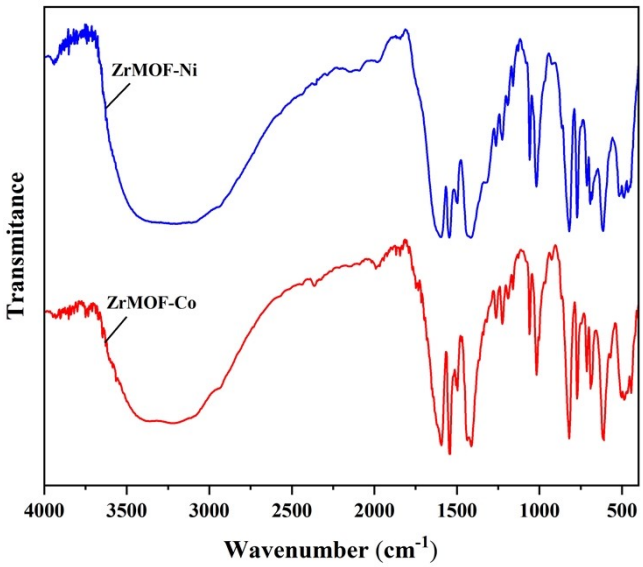

Figure S5. IR spectra of **ZrMOF-Co and ZrMOF-Ni.**

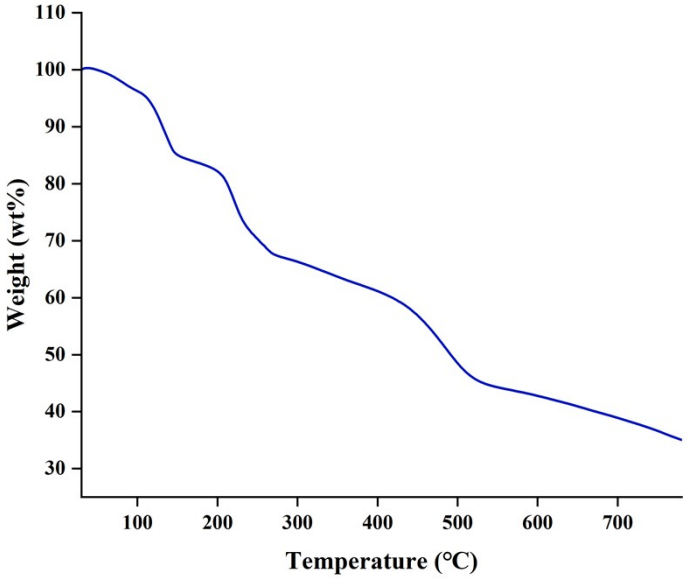

Figure S6. TGA curve of **ZrMOF-Co.**

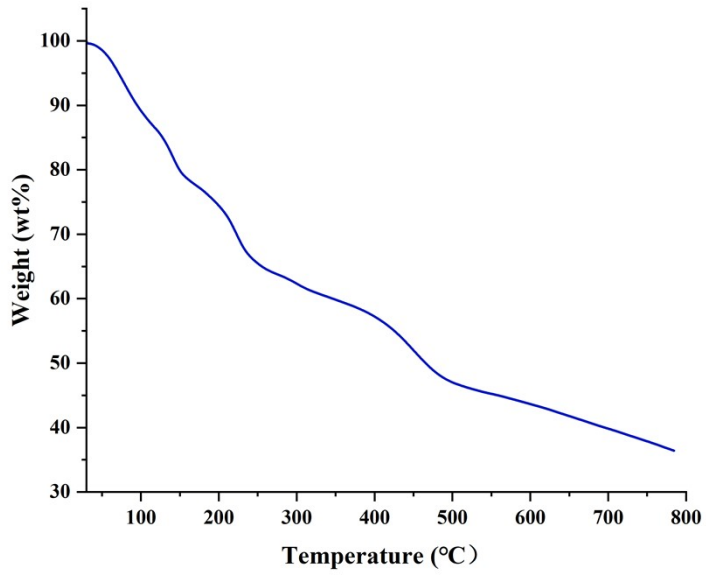

Figure S7. TGA curve of **ZrMOF-Ni**.

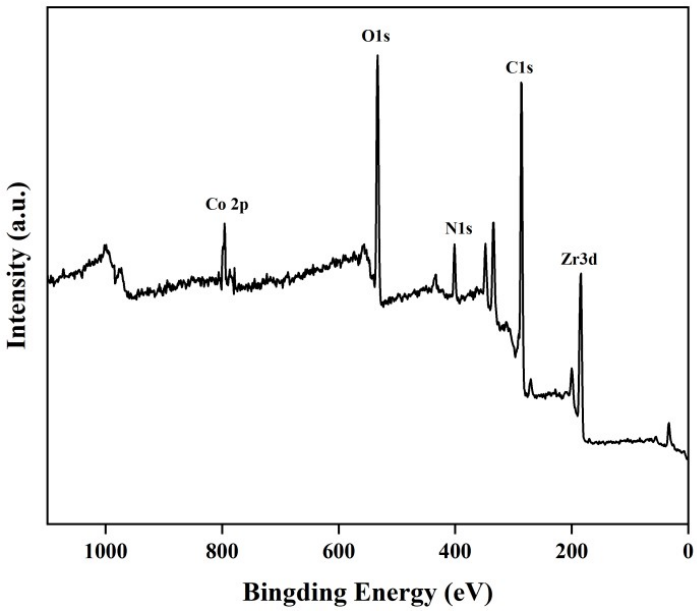

Figure S8. XPS spectra of ZrMOF-Co.

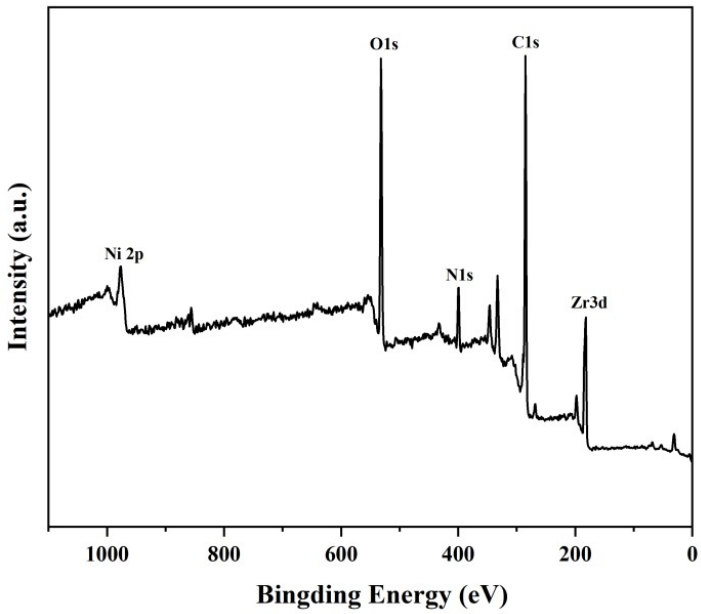

Figure S9. XPS spectra of ZrMOF-Ni.

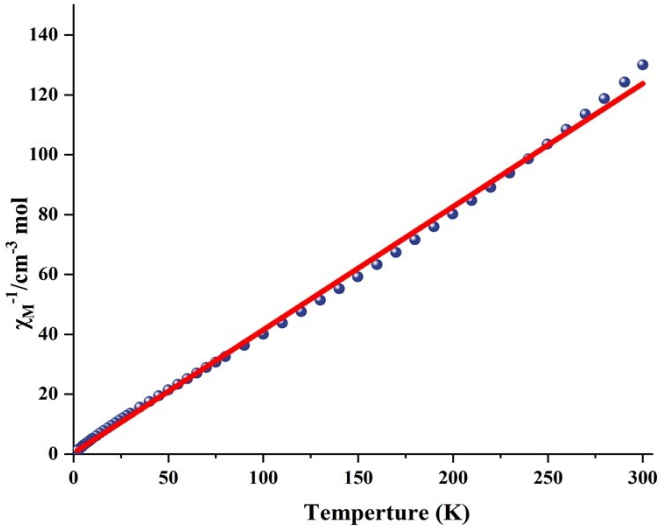

Figure S10. The temperature dependence of the inverse magnetic susceptibility χ_M^{-1} for **ZrMOF-Co** between 2 and 300 K. The solid red line was generated from the best fit by the Curie-Weiss expression in the range of 0-300 K with the Curie constant C = 2.43 cm^3 K mol^{-1} and the Weiss constant $\theta = -0.79$ K.

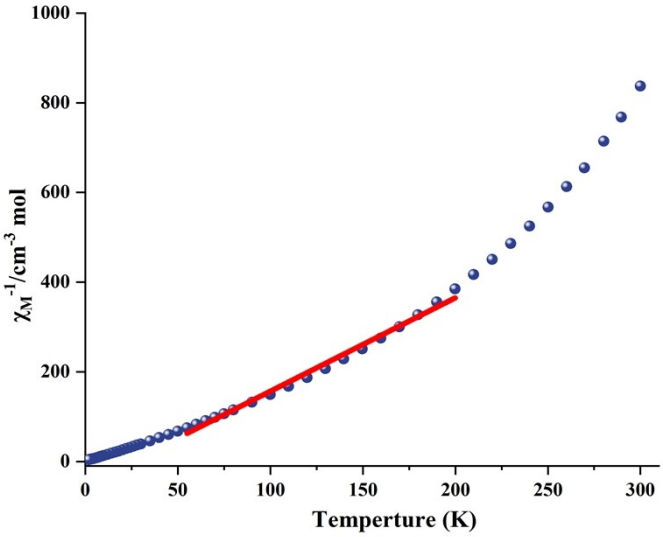

Figure S11. The temperature dependence of the inverse magnetic susceptibility $\chi_{M^{-1}}$ for **ZrMOF-Ni** between 2 and 300 K. The solid red line was generated from the best fit by the Curie-Weiss expression in the range of 55–200 K with the Curie constant C = 0.48 cm^3 K mol^{-1} and the Weiss constant θ = 24.84 K.

References:

[1] V. Guillerm, S. Gross, C. Serre, T. Devic, M. Bauer and G. Férey. Chem Commun., 2010, **46**, 767-769.

[2] P. Deria, W. Bury, I. Hod, C. Kung, O. Karagiaridi, J. Hupp and O. Farha, Inorg. Chem., 2015, **54**, 2185–2192

[3] Yuan, J. Qin, J. Su, B. Li, J. Li, W. Chen, Hannah F. Drake, P. Zhang, D. Yuan, J. Zuo and H. Zhou, Angew Chem Int Edit., 2018, **57**, 12578-12583.

[4] C. Tan, X. Han, Z. Li, Y. Liu and Y, Cui, J Am Chem Soc., 2018, **140**, 16229-16236.

[5] C. Chen, Z. Wei, Y. Fan, P. Su, Y. Ai, Q. Qiu, K. Wu, S. Yin, M. Pan and C. Su. Chem., 2018, **4**, 2658-2669.

[6] S. Yuan, L. Li, K. Wang, S. Gregory, P. Zhang, Y. Wang and H. Zhou, ACS Cent. Sci., 2018, **4**, 1719–1726.

[7] L. Zhang, S. Yuan, L. Feng, B. Guo, J. Qin, B. Xu, C. Lollar, D. Sun and H. Zhou, Angew Chem Int Edit, 2018, **57**, 5095-5099.

[8] L. Feng, S. Yuan, J. Qin, Y. Wang, A. Kirchon, D. Qiu, L. Cheng, S. T. Madrahimov and H. Zhou. Matter, 2019, **1**, 156-167.

[9] S. Yuan, J. Peng, Y. Zhang and Y. Shao-Horn, J. Phys. Chem. C., 2019, **123**, 28266-28274.

[10] M. Zhao, J. Chen, B. Chen, X. Zhang, Z. Shi, Z. Liu, Q. Ma, Y. Peng, C. Tan, X. Wu and H. Zhang., J. Am. Chem. Soc. 2020, 142, **19**, 8953–8961

[11] W. Gong, H. Arman, Z. Chen, Y. Xie, F. Son, H. Cui, X. Chen, Y. Shi, Y. Liu, B. Chen, O. Farha and Y. Cui, J. Am. Chem. Soc. 2021, **143**, 657-663.

[12] M. Maity, P. Howlader, S. Mukherjee, Cryst Growth Des., 2018, **18**, 6956-6964.